In situ electric field induced domain evolution in Ba(Zr0.2Ti0.8)O3-0.3(Ba0.7Ca0.3)TiO3 ferroelectrics

M. Zakhozheva, L. A. Schmitt, M. Acosta, W. Jo, J. Rödel, and H.-J. Kleebe

Citation: Applied Physics Letters **105**, 112904 (2014); doi: 10.1063/1.4896048

View online: http://dx.doi.org/10.1063/1.4896048

View Table of Contents: http://scitation.aip.org/content/aip/journal/apl/105/11?ver=pdfcov

Published by the AIP Publishing

In situ electric field induced domain evolution in $Ba(Zr_{0.2}Ti_{0.8})O_3$-0.3$(Ba_{0.7}Ca_{0.3})TiO_3$ ferroelectrics

M. Zakhozheva,[1] L. A. Schmitt,[2] M. Acosta,[2] W. Jo,[3] J. Rödel,[2] and H.-J. Kleebe[1]
[1]*Institute of Applied Geosciences, Technische Universität Darmstadt, Schnittspahnstraße 9, 64287 Darmstadt, Germany*
[2]*Institute of Materials Science, Technische Universität Darmstadt, Alarich-Weiss-Str. 2, 64287 Darmstadt, Germany*
[3]*School of Materials Science and Engineering, Ulsan National Institute of Science and Technology, Ulsan 689-798, South Korea*

(Received 6 August 2014; accepted 7 September 2014; published online 17 September 2014)

In this work, the lead-free $Ba(Zr_{0.2}Ti_{0.8})O_3$-0.3$(Ba_{0.7}Ca_{0.3})TiO_3$ piezoelectric ceramic was investigated *in situ* under an applied electric field by transmission electron microscopy. Significant changes in domain morphology of the studied material have been observed under an applied electric field. During the poling process, the domain configurations disappeared, forming a single-domain state. This multi- to single-domain state transition occurred with the formation of an intermediate nanodomain state. After removing the electric field, domain configurations reappeared. Selected area electron diffraction during electrical poling gave no indication of any structural changes as for example reflection splitting. Rather, a contribution of the extrinsic effect to the piezoelectric response of the $Ba(Zr_{0.2}Ti_{0.8})O_3$-0.3$(Ba_{0.7}Ca_{0.3})TiO_3$ was found to be dominant. [http://dx.doi.org/10.1063/1.4896048]

Today, lead-based piezoelectric ceramics with perovskite structure, such as lead-zirconium-titanate (PZT), are widely used in various ferroelectric and piezoelectric applications such as sensors and actuators because of their superior piezoelectric (with piezoelectric constant, $d_{33} = 500$–600 pC/N), dielectric, and mechanical properties.[1] Nevertheless, because of lead toxicity,[2] it is necessary to search for a suitable lead-free alternative for these materials. During the last few decades, numerous investigations have been presented on Pb-free piezoceramics. First viable contenders and products are now appearing at the marketplace.[3–5] However, the properties of most lead-free materials are still lower in comparison to PZT.[6–8] Thus, development of lead-free piezoelectric ceramics is of great interest.

In 2009, Liu and Ren reported a lead-free $Ba(Zr_{0.2}Ti_{0.8})O_3$-x$(Ba_{0.7}Ca_{0.3})TiO_3$ (abbreviated as BZT-xBCT) ferroelectric system, which exhibits impressive piezoelectric properties ($d_{33} = 620$ pC/N), comparable to PZT.[9] They proposed a phase diagram with temperature dependent polymorphic phase transitions (PPT) separating rhombohedral and tetragonal phases, where the piezoelectric and dielectric properties peak.[9] The phase diagram is characterized by the existence of a triple point at which cubic, rhombohedral, and tetragonal phases coexist, at $x = 0.32$ and at $T = 57\,^{\circ}C$. Liu and Ren attributed the high piezoelectricity of the system to the enhanced polarization rotation around the triple point and PPT.[9] However, according to recent studies, the phase diagram of the BZT-xBCT system is much more complex than initially reported by Liu and Ren.[10–12] Keeble *et al.* by means of synchrotron diffraction studies revealed the existence of a bridging orthorhombic phase between the rhombohedral and tetragonal ones.[11] Instead of a triple point, they observed a phase convergence region, where rhombohedral, tetragonal, orthorhombic, and cubic phases are hardly distinguishable experimentally. These results were supported by Tian *et al.*[10] Nevertheless, it was already shown phenomenologically that two triple points may exist in a very narrow temperature and compositional range.[13] It should be highlighted that the interleaving region between rhombohedral and tetragonal symmetries may also consist of rhombohedral and tetragonal phase coexistence, as proposed in different detailed structural studies.[14–17] Its presence has been shown by several experimental techniques such as Raman, thermally stimulated depolarization currents, and elastic and dielectric properties.[18–20] Moreover, regardless of its nature, Acosta *et al.*[12] have demonstrated that it is also characterized by enhanced electromechanical properties.

In order to rationalize the properties of the ferroelectric ceramics, intrinsic and extrinsic contributions need to be assessed.[21] Intrinsic contributions are associated with field induced lattice deformation, while domain wall movement under an external electric field characterizes the extrinsic effect.[21,22]

Acosta *et al.* investigated the intrinsic and extrinsic contribution to the properties of a large variety of BZT-xBCT composition as a function of temperature.[12] The maximum polarization was observed at the phase convergence region while the maximum piezoelectric coefficients were detected at the ferroelectric-ferroelectric phase transition region. It was proposed that the polarization rotation is enhanced around the triple point and PPT, but the ability of the system to retain its spontaneous polarization determines the final intrinsic properties. Therefore, maximum small signal d_{33} values are observed only at the orthorhombic to tetragonal PPT and not at the convergence region. On the other hand, extrinsic contributions peaking around the PPTs were rationalized with a broad minimum in energy barrier,[23] leading to alleviated domain switching.[24] An increased value of the intrinsic piezoelectric coefficient at the ferroelectric-ferroelectric phase transition regions was also observed by Gao *et al.*,[25] while the

extrinsic piezoelectric response showed a peak at the phase instability region with the highest contribution of 67% for BZT-0.5BCT system. They concluded that the higher contribution to the piezoelectric properties of BZT-xBCT piezoceramics is from the extrinsic effect.

It was proposed that strong piezoelectricity in the BZT-xBCT corresponds well with the miniaturization of domains.[14] The microstructural features of the BZT-xBCT were studied by Gao *et al.*[14,17] The BZT-0.5BCT, which lies at the PPT and exhibits enhanced piezoelectric properties,[9] showed a unique domain microstructure. Within micro-sized domains nanodomains with the average size of 20–100 nm were visible, which is an indication of free energy degeneracy.[13,26]

Guo *et al.* performed *in situ* electric field transmission electron microscopy (TEM) experiments on BZT-0.5BCT.[27] A reversible multi-domain to single-domain transition at moderate poling fields was reported. They suggested that the appearance of such single-domain state, which is believed to have orthorhombic symmetry, is the reason of the high piezoelectric properties in the BZT-0.5BCT system. Nevertheless, it is still unclear whether the mono-domain state is intimately related to the triple point, the phase convergence region or can also occur at a considerable distance to the PPT in this system. Therefore, we chose BZT-0.3BCT composition for this study as representative material, which locates deep in the rhombohedral region of the phase diagram.[9,11,12] In order to assess the field-dependent domain state, poling induced changes in the domain morphology of $Ba(Zr_{0.2}Ti_{0.8})O_3$-$0.3(Ba_{0.7}Ca_{0.3})TiO_3$ piezoelectric ceramic were characterized *in situ* using TEM.

$Ba(Zr_{0.2}Ti_{0.8})O_3$-$0.3(Ba_{0.7}Ca_{0.3})TiO_3$ (abbreviated as BZT-0.3BCT) ceramics were synthesized using a conventional solid-state reaction route from oxides and carbonate powders of $BaCO_3$ (purity 99.8%), ZrO_2 (purity 99.5%), TiO_2 (purity 99.6%), and $CaCO_3$ (purity 99.5%). Mixed powders were calcined at 1300 °C for 2 h and sintered at 1500 °C for 2 h. Further information on specimen synthesis can be found elsewhere.[12,23]

Samples for TEM investigation were ultrasonically cut into discs of 3 mm in diameter, mechanically thinned to a thickness of about 140 μm by tripod polishing and then dimpled to a final thickness of about 20 μm by a Gatan Model 656 Dimple Grinder. The samples were annealed at 450 °C for 2 h in order to minimize induced stresses during preparation. Finally, they were thinned by ion milling with Argon ions. Gold electrodes with a spacing of 120 μm were evaporated on top of the sample and contacted with the *in situ* electric field holder Gatan Model 646. *In situ* TEM experiments were performed using a CM20 (FEI, Eindhoven, The Netherlands) instrument operated at 200 kV. Part of the experiment (2nd and 3rd cycle) was recorded with a CCD camera. Applied nominal maximum voltage was ±5 kV/cm. The video was processed and can be seen at the homepage of this journal (Fig. 1 (multimedia view)).

The grain morphology of BZT-0.3BCT at the initial state is depicted in Fig. 2. Lamellar domains with needle shaped domain tips are visible inside the majority of grains (Fig. 2(a)). However, grains with homogeneous contrast were also observed. Fig. 2(b) shows a grain orientated along the $[1–31]_c$ zone axis. Clearly, no domain structure is visible.

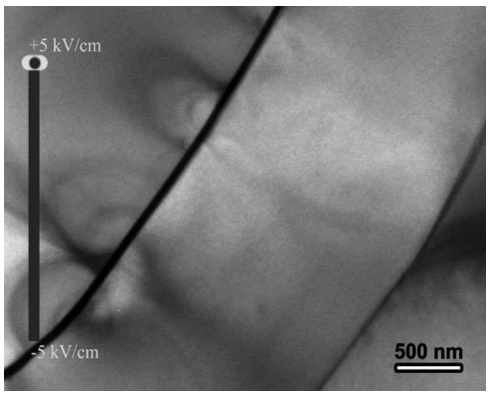

FIG. 1. TEM bright field image of the BZT-0.3BCT showing three adjacent grains at an electric field of +5 kV/cm. A single-domain state is present within each grain. Strain contrast is visible at the grain boundary. (multimedia view) [URL: http://dx.doi.org/10.1063/1.4896048.1]

The corresponding selected area electron diffraction (SAED) pattern does not reveal any reflection splitting (Fig. 2(b), inset).

The grain orientated along $[1–53]_c$ zone axis was used to analyze the domain structure evolution during electrical poling (Fig. 3). Prior to applying an electric field lamellar domain walls with traces along [30–1] direction were observed inside the grain (Fig. 3(a)). These domain walls are expected to be (10–1) type walls, which are tilted about 13.8° with respect to the viewing direction. This corresponds to the presence of 109° domains reported for rhombohedral PZT.[28] TEM bright field image recorded at a field of 3.3 kV/cm do not provide any detectable changes in domain morphology (Fig. 3(b)). At the nominal poling field of 5 kV/cm, all domain walls disappeared, forming a single-domain state throughout the grain (Fig. 3(c)). Thus, an electric field induced transformation from the multi-domain to the single-domain state occurred at moderate poling fields. This transformation is found to be reversible, since multi-domain contrast reappears inside the grains upon field removal. Fig. 3(d) illustrates the SAED pattern recorded prior to applying a poling field. The SAED pattern is devoid of reflection splitting and detectable changes during electrical poling.

A grain imaged along [1–14] zone axis is depicted in Fig. 4. At zero field edge-on 109° domains with walls in (1–10) planes and domain walls tracing along ⟨311⟩ direction, which lie along {110} planes are visible inside the grain. Increasing the poling field to 2.5 kV/cm, lamellar domains grow,

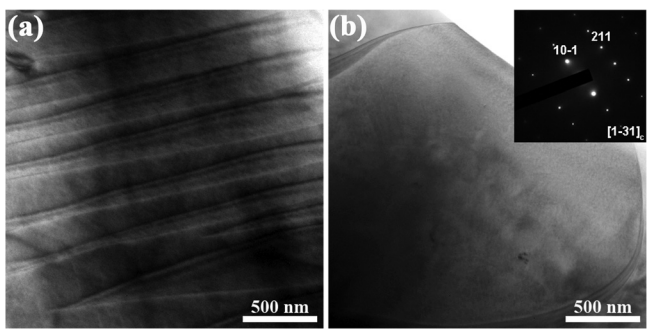

FIG. 2. TEM bright field images of the BZT-0.3BCT. (a) Domain contrast is visible inside the grain. (b) Grain orientated along the $[1\text{-}31]_c$ zone axis reveals a homogeneous contrast. The inset depicts the SAED pattern.

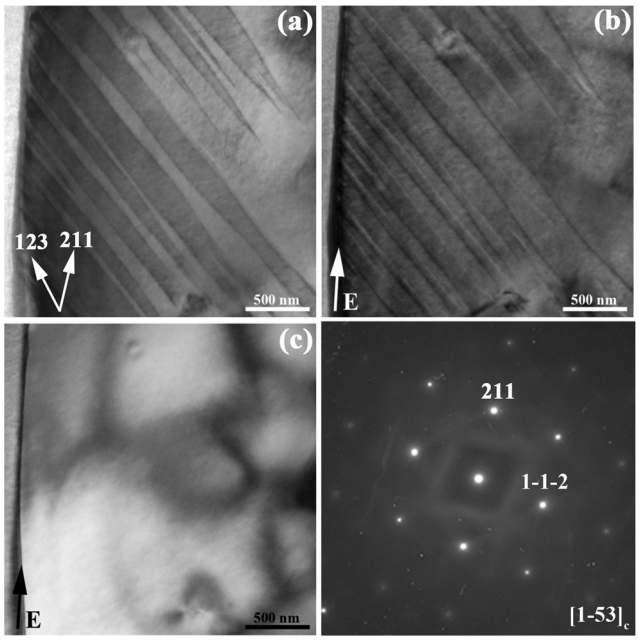

FIG. 3. In situ TEM bright field images of the BZT-0.3BCT along the $[1–53]_c$ zone axis at (a) zero field, (b) 3.3 kV/cm, and (c) 5 kV/cm. The direction of the poling field is indicated by the arrow. (d) Corresponding SAED pattern at zero field.

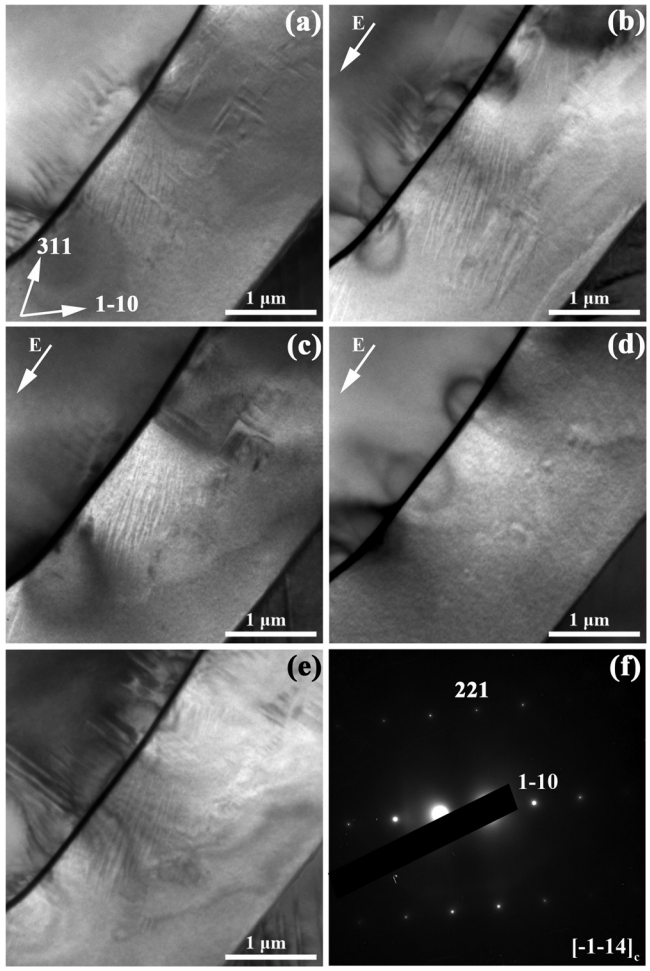

FIG. 4. In situ TEM bright field images of BZT-0.3BCT along the [11–4]c zone axis at (a) zero field, (b) 2.5 kV/cm, (c) 4.2 kV/cm, (d) 5 kV/cm, and (e) zero field after two cycles. (f) The SAED pattern at 5 kV/cm. The direction of the poling field is indicated by the arrow.

indicating a field induced domain switching. At the nominal field of 4.2 kV/cm, the domain size decreased and when the poling field reached the value 5 kV/cm the transition from the multi- to single-domain state, which is found to be reversible, occurred (Figs. 4(a)–4(d)). During the second cycle same region was monitored by CCD (Fig. 1 (multimedia view)). At approximately +3 kV/cm, the domains vanished. At higher fields a single domain state was formed and strain contrast at the grain boundary was visible. The domains reappeared when the field was reduced to +3 kV/cm. Several domain configurations developed as a function of electric field and a single domain state was reached beyond −3 kV/cm. In the 3rd cycle, a domain configuration of an adjacent grain was monitored. Wedge shaped domains with a nanodomain contrast are visible. Approaching +3 kV/cm, the nanodomain contrast increased. The domains disappeared at +5 kV/cm. In the remaining 3rd cycle, the three grains were monitored again.

The reported single-domain state was observed in several studied grains under poling conditions. It should be noted that a further increase of the poling field lead to a multi-domain state formation. However, during poling no visible changes in the SAED pattern were observed. Moreover, prior to a single-domain state a nucleation of nanometer-sized domains within lamellar microdomains occurred. The scheme with three individual grains depicted in Fig. 5 was designed to visualize the domain evolution during the poling process. According to our results, an increase of the poling field leads to the multi-domain state (A) → nanodomain state → single-domain state transformations, which are reversible. During the single-domain state, however, when the electric field is further increased, the multi-domain state (B) is formed. Further cycling enables switching between two different multi-domain states (Fig. 5).

A single-domain state under poling conditions was observed by Guo *et al.* for polymorphic phase boundary composition BZT-0.5BCT as well and believed to be the main reason for the excellent piezoelectric properties of this system.[27] They observed a multi- to single-domain transformation at moderate fields. Further increase of the poling field resulted in the reappearance of multiple domain configurations.

However, the performed *in situ* electric field studies on BZT-0.3BCT showed that a poling induced single-domain state is not an exclusive characteristic feature of the polymorphic phase boundary composition BZT-0.5BCT. The BZT-0.3BCT piezoelectric ceramic, which has rhombohedral crystal symmetry at room temperature,[9,11,12] also showed an electric field induced reversible transformation from multi- to single-domain state with appearance of an intermediate nanodomain state. The intermediate nanodomain state facilitated domain switching under the applied electric field and hence the poling process. It should be noted that a comparable scenario was observed both in PLZT[29] as well as in PZT.[30] In one case, the nanodomains appeared during switching,[29] whereas in the other case, they were already present in the initial state.[30] Under the applied electric field, the nanodomain configuration changed, leading to the conclusion that

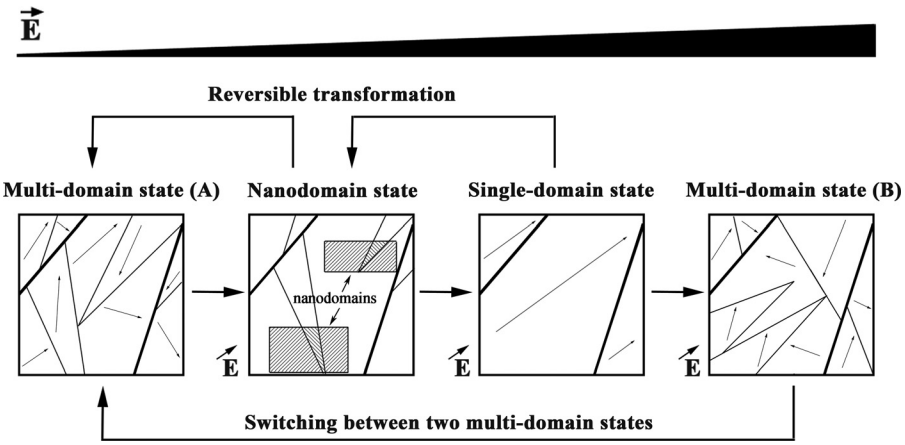

FIG. 5. Scheme of the domain evolution as a function of electric field. An increase in electric field leads to multi-domain state (A) → nanodomain state → single-domain state transformations, which are reversible. Increase of the electric field within the single-domain state leads to a multi-domain state (B). Further cycling enables switching between two different multi-domain states.

the extrinsic contribution to the inverse piezoelectric effect is closely related to the existence of nanodomains.

In the present study, a field-induced transformation from a multi- to a single-domain state was monitored in BZT-0.3BCT, which is far away from the polymorphic phase boundary. The displacement of the domain walls and changes in the domain configuration during poling indicated a high extrinsic contribution to the piezoelectric properties in BZT-0.3BCT piezoceramic.

This work was supported by the Deutsche Forschungsgemeinschaft, Sonderforschungsbereich 595, and by the AdRIA Hesse State Center for Adaptronics. We are grateful for helpful discussions with Xiaoli Tan, Cheng Ma, and Hanzheng Guo.

[1]B. Jaffe, W. R. Cook, and H. Jaffe, *Piezoelectric Ceramics* (Academic Press Inc., 1971).
[2]EU-Directive 2011/65/EU, Off. J. Eur. Union L 174:88 (2011).
[3]T. Tou, Y. Hamaguti, Y. Maida, H. Yamamori, K. Takahashi, and V. Terashima, Jpn. J. Appl. Phys. **48**, 07GM03 (2009).
[4]Y. Doshida, H. Shimizu, Y. Mizuno, and H. Tamura, Jpn. J. Appl. Phys. **52**, 07HE01 (2013).
[5]W. Krauss, D. Schütz, M. Naderer, D. Orosel, and K. Reichmann, J. Eur. Ceram. Soc. **31**(9), 1857 (2011).
[6]T. Takenaka, H. Nagata, Y. Hiruma, Y. Yoshii, and K. Matumoto, J. Electroceram. **19**(4), 259 (2007).
[7]J. Rödel, W. Jo, K. T. P. Seifert, E.-M. Anton, T. Granzow, and D. Damjanovic, J. Am. Ceram. Soc. **92**(6), 1153 (2009).
[8]Y. Saito, H. Takao, T. Tani, and T. Nonoyama, Nature **432**, 84 (2004).
[9]W. Liu and X. Ren, Phys. Rev. Lett. **103**(25), 257602 (2009).
[10]Y. Tian, L. Wei, X. Chao, Z. Liu, and Z. Yang, J. Am. Ceram. Soc. **96**(2), 496 (2013).
[11]D. S. Keeble, F. Benabdallah, P. A. Thomas, M. Maglione, and J. Kreisel, Appl. Phys. Lett. **102**(9), 092903 (2013).
[12]M. Acosta, N. Novak, W. Jo, and J. Rödel, Acta. Mater. **80**, 48 (2014).
[13]A. A. Heitmann and G. A. Rossetti, J. Am. Ceram. Soc. **97**(6), 1661 (2014).
[14]J. Gao, D. Xue, Y. Wang, D. Wang, and L. Zhang, Appl. Phys. Lett. **99**(9), 092901 (2011).
[15]M. C. Ehmke, S. N. Ehrlich, J. E. Blendell, and K. J. Bowman, J. Appl. Phys. **111**(12), 124110 (2012).
[16]A. Bjørnetun Haugen, J. S. Forrester, D. Damjanovic, B. Li, K. J. Bowman, and J. L. Jones, J. Appl. Phys. **113**, 014103 (2013).
[17]J. Gao, L. Zhang, D. Xue, T. Kimoto, M. Song, L. Zhong, and X. Ren, J. Appl. Phys. **115**(5), 054108 (2014).
[18]F. Benabdallah, A. Simon, H. Khemakhem, C. Elissalde, and M. Maglione, J. Appl. Phys. **109**(12), 124116 (2011).
[19]D. Damjanovic, A. Biancoli, L. Batooli, A. Vahabzadeh, and J. Trodahl, Appl. Phys. Lett. **100**(19), 192907 (2012).
[20]D. R. J. Brandt, M. Acosta, J. Koruza, and K. G. Webber, J. Appl. Phys. **115**(20), 204107 (2014).
[21]D. Damjanovic, Rep. Prog. Phys. **61**, 1267 (1998).
[22]M. J. Hoffmann, M. Hammer, A. Endriss, and D. C. Lupascu, Acta mater. **49**(7), 1301 (2001).
[23]S. Zhukov, Y. A. Genenko, M. Acosta, H. Humburg, W. Jo, J. Rödel, and H. von Seggern, Appl. Phys. Lett. **103**(15), 152904 (2013).
[24]G. Tutuncu, B. Li, K. Bowman, and J. L. Jones, J. Appl. Phys. **115**, 144104 (2014).
[25]J. Gao, X. Hu, L. Zhang, F. Li, L. Zhang, Y. Wang, Y. Hao, L. Zhong, and X. Ren, Appl. Phys. Lett. **104**(25), 252909 (2014).
[26]G. A. Rossetti and A. G. Khachaturyan, Appl. Phys. Lett. **91**(7), 072909 (2007).
[27]H. Guo, C. Zhou, X. Ren, and X. Tan, Phys. Rev. B **89**(10), 100104 (2014).
[28]J. Ricote, R. W. Whatmore, and D. J. Barber, J. Phys.: Condens. Matter **12**, 323 (2000).
[29]S. Schaab and T. Granzow, Appl. Phys. Lett. **97**(13), 132902 (2010).
[30]R. Theissmann, L. A. Schmitt, J. Kling, R. Schierholz, K. A. Schönau, H. Fuess, M. Knapp, H. Kungl, and M. J. Hoffmann, J. Appl. Phys. **102**(2), 024111 (2007).